Motional Perturbation at the Microphase Boundary in Thermoplastic Elastomers

J. Denault, B. Morèse-Séguéla, R. Séguéla, and J. Prud'homme*

Department of Chemistry, University of Montreal, Montreal, Quebec, Canada H3C 3V1

Received November 3, 1989; Revised Manuscript Received January 31, 1990

ABSTRACT: ^{13}C NMR spin–lattice relaxation times, T_1, and nuclear Overhauser enhancement factors, NOEF, have been measured at two Larmor frequencies (20.1 and 100.6 MHz) and over a range of temperatures (40–100 °C) for the polyisoprene (PI) microphase in poly(styrene-*b*-isoprene) (SI) diblock polymers having a lamellar morphology. The study was carried out over a wide range of molecular weights (or lamella thicknesses) in order to scrutinize the effect of the microdomain boundary upon the dynamics of the PI chains. It is shown that the perturbation of the high-frequency segmental motion probed by T_1 and NOEF is limited to a zone of finite thickness (3.6 nm) near the microphase interface. This perturbation is characterized by a twofold increase in correlation time for segmental motion together with a significant increase in motional dispersion or cooperativity. Contrary to ^{13}C NMR line widths and glass transition temperature ($T_{g,I}$) of the PI microphase, which both increase with decreasing lamellar thickness in the range below 3.6 nm, T_1 and NOEF exhibit an asymptotic behavior in this range. T_1 and NOEF are also independent of the PS microphase rigidity. These features provide evidence that the changes in the PI chain dynamics probed by these parameters are mainly due to chain end immobilization rather than to change in free volume near the microphase boundary.

Introduction

Microphase separation in two-component block polymers is a well-known phenomenon that yields mesomorphic structures in which the dissimilar components form ordered microdomains linked together by covalent bonds.[1] The size of the microdomains is governed by the length of the individual blocks, while their morphology depends upon both the volume fraction of the components and the specimen preparation conditions.[2] An important technological development based upon this phenomenon is indubitably that of the so-called thermoplastic elastomers, a class of material in which discrete glassy or crystalline microdomains provide physical cross-linking to a rubbery matrix.[3] Although many fundamental questions related to microphase separation and microdomain formation in block copolymers have been clarified, little is known concerning chain dynamics in these materials. In that respect, special attention should be given to systems comprising rubbery and glassy microphases. Indeed, particularly important for these systems would be to examine whether a significant transfer of kinetic energy occurs through the covalent bonds at the interface between the rubbery and the rigid microphase. Also important would be to clarify to what extent the immobilization of the rubbery chain ends at the microdomain interface may affect chain motion in the core of the rubbery microphase. Better knowledge of these points might contribute enlightenment on structure–property relationships in thermoplastic elastomers and also in other phase-separated systems such as filled elastomers and high-impact polymer blends.

High-resolution ^{13}C NMR spin relaxation techniques are among the most sensitive and discriminating approaches for probing molecular motion in polymers. Not only do these techniques allow the study of chain dynamics at the level of each individual ^{13}C nuclei, they also offer a variety of experiments suitable for discriminating phases of different composition in bulk materials. For instance, liquid-state high-resolution ^{13}C NMR relaxation studies may be made directly on bulk elastomers at temperatures well above their glass transition temperature (T_g).[4-9] In the case of block polymers, this approach allows a selective investigation of the rubbery microphase without any spectral interference due to the rigid microphase.[10,11] In turn, for situations in which the dissimilar components are partially miscible, spectra measured by the liquid-state approach might be useful to detect the presence of the second component in the rubbery microphase. On the other hand, solid-state high-resolution ^{13}C NMR techniques might be useful to discriminate chain segments of low mobility that do not contribute to the liquid-state spectra. This could include rubbery segments dissolved within the glassy microphase or located close to the interface boundary in either microphase.

The present paper describes a ^{13}C NMR investigation performed on a series of monodisperse poly(styrene-*b*-isoprene) (SI) diblock polymers having the same styrene weight fraction ($w_S = 0.50$) but number-average molecular weights, M_n, ranging from 5×10^3 to 4×10^5. The aim of this work was to examine the chain dynamics over a wide range of lamella thicknesses (or interfacial areas) in polyisoprene (PI) microdomains of well-defined lamellar morphology. For that purpose, spin–lattice relaxation times, T_1, and nuclear Overhauser enhancement factors, NOEF, were measured by means of the usual liquid-state techniques over a temperature range (40–100 °C) well above the T_g's of the PI microdomains. The relaxation data were interpreted in terms of correlation times for segmental motion by means of two different approaches. In the first approach, use was made of the recent physical model for chain dynamics proposed by Dejean de la Batie et al.[6] In the second approach, the PI backbone motion was modeled on the basis of a log χ^2 empirical distribution function of isotropic rotors.[4] In each case, the correlation times for segmental motion were determined by fitting the model to the methylene T_1 data measured at two well-separated Larmor frequencies (20.1 and 100.6 MHz). In turn, the NOEF data (measured at 20.1 MHz only) were used for testing the model relevancy. Also examined was the variation of the PI line widths as a function of the lamella thickness.

In order to make a founded interpretation of the NMR data, special attention was given to fully characterize the structural and physical features of the microphases in the present materials. Morphology and microdomain sizes were determined by small-angle X-ray scattering (SAXS),

0024-9297/90/2223-4658$02.50/0 © 1990 American Chemical Society

Table I
Styrene Weight Fractions (w_S), Number-Average Molecular Weights (M_n), and Polydispersity Indexes (M_w/M_n) of the Block Polymers and Lamellar Thicknesses (t_I and t_S), and Glass Transition Temperatures ($T_{g,I}$ and $T_{g,S}$) of the PI and PS Microdomains

sample	w_S[a]	$10^{-3}M_n$	M_w/M_n	t_I, nm	t_S, nm	$T_{g,I}$, °C	$T_{g,S}$, °C
SI-5k	0.51	4.85	1.03	(3.85)[b]	(3.45)	−49	3
SI-8k	0.50	8.2	1.02	(5.27)[b]	(4.43)	−54	31
SI-13k	0.50	12.6	1.04	7.16	6.14	−58	65
SI-32k	0.49	31.7	1.05	14.0	11.5	−60	93
SI-95k	0.48	94.7	1.09	30.3	24.0	−60	104
SI-220k	0.50	221	1.09	52.2	44.8	−61	106
SI-380k	0.48	380	1.13	(79)[c]	(63)	−60	107

[a] Determined by ^{1}H NMR spectroscopy. [b] Based on the single SAXS peak observed for samples SI-5k and SI-8k. [c] Estimated by extrapolation on the data curve of Figure 2.

and microphase T_g's were measured by differential scanning calorimetry (DSC). The possibility of partial miscibility in the case of the low molecular weight materials was investigated by liquid- and solid-state ^{13}C NMR spectroscopy. The results of these investigations are presented at the beginning of this paper together with a two-phase physical model that accounts for the variation of the microphase T_g's as a function of the lamella thickness.

Experimental Section

Materials. The SI and homo-PI samples were prepared by anionic polymerization by using *sec*-butyllithium as initiator and benzene as solvent. The microstructure of the PI blocks was identical with that of the homo-PI chains. As determined from the relative intensities of the methyl resonances[9] in 100.6-MHz proton-decoupled ^{13}C NMR spectra measured on the bulk at 100 °C, it was 71% cis-1,4, 22% trans-1,4, and 7% 3,4. In order to avoid oxidative degradation of the PI blocks, all the samples were stored at −20 °C in vacuum-sealed tubes. Number-average molecular weights, M_n, were determined by either membrane osmometry in toluene or tonometry in benzene. Polydispersity indexes, M_w/M_n, were characterized by size exclusion chromatography in toluene, by using a series of three Ultrastyragel columns calibrated with polystyrene standards. This method also provided quantitative data concerning the good stability of the materials over the years of the present study. Glass transition temperatures, T_g, were measured at a heating rate of 40 °C/min with a Model DSC-4 Perkin-Elmer calorimeter flushed with dry helium. Temperature calibrations were made with standard materials having melting points in the range −69 to +156 °C. Specimens were annealed at 125 °C many days prior to the DSC measurements.

Small-Angle X-ray Scattering Measurements. SASX patterns were recorded on photographic films with a Model 2202 Rigaku-Denki goniometer provided with a two-pinhole collimator. Ni-filtered Cu Kα radiation (λ = 0.154 nm) was generated by a Philips tube operated at 40 kV and 20 mA. The second pinhole (0.2-mm diameter), specimen, and photographic film were placed 300, 320, and 630 mm from the first pinhole (0.3-mm diameter), respectively. Two SI samples at the lower end of the molecular weight range were rubbery ($M_n = 8.2 \times 10^3$) and viscous ($M_n = 4.8 \times 10^3$) materials at room temperature. Their SAXS patterns were recorded by using 2-mm-thick cells fitted with Mylar windows. The other samples were rigid materials. They were examined under the form of film specimens about 0.8 mm thick prepared by solvent evaporation (toluene) over a mercury bed. These specimens were dried under high vacuum and subsequently annealed for a period of 5 h at a temperature 20 °C above the T_g of their polystyrene microphase. All samples yielded circular SAXS patterns. The radial profile of the scattering intensity was recorded from the photographic films by means of a Joyce-Loebl microdensitometer.

^{13}C NMR Measurements. T_1 measurements at 20.1 and 100.6 MHz were carried out under scalar decoupling with Bruker Model WP-80 and WH-400 spectrometers, respectively. Use was made of the standard inversion–recovery Fourier transform technique (IRFT). The SI rigid samples were heat molded into the form of annular cylinders and slipped into 10-mm-diameter NMR tubes. The viscous or rubbery samples were allowed to flow into the bottom of 10-mm tubes by heating the tubes at 90 °C in an oil bath. In both cases, a vacuum-sealed 5-mm NMR tube containing a 1:1 mixture of D_2O and ethylene glycol was inserted concentrically in the 10-mm NMR tubes. This external mixture provided deuterium lock for field stability and chemical shift reference. Signal intensities, S_t, were measured for at least 10 values of the relaxation delay time, t, in the range 0–1.5 T_1. As usual, T_1 was computed from the inverse of the least-squares slope of ln $(S_\infty - S_t)$ as a function of t. The pulse repetition period was longer than 5 T_1. Nuclear Overhauser enhancements, (NOEF + 1), were determined from the intensity ratios of scalar-decoupled and inverse-gated-decoupled spectra. The instrumental adjustments concerning T_1 and NOEF measurements are quoted in the former paper on homo-PI.[9] Reproducibility of T_1 was better than 5% while that of NOEF was ca. ±0.05.

Dipolar-decoupled CP-MAS solid-state ^{13}C NMR spectra were recorded at 75.4 MHz with a Varian Model VXR-300 spectrometer provided with a Doty Scientific probe. The solid specimens were heat molded and inserted in 7-mm-diameter sapphire rotors fitted with Kel-F turbine caps. The spectra were recorded at room temperature with various cross-polarization contact times in the range 0.05–9 ms. Spinning rate was 4.7 kHz. Power levels were 55 kHz for dipolar decoupling and 38 kHz for cross polarization. Spectral width, acquisition time, pulse width, and pulse repetition period were 30 kHz, 0.067 s, 90°, and 3 s, respectively.

Results and Discussion

Morphology, Microdomain Sizes, and Glass Transition Behavior of the SI Materials. The molecular characteristics of the SI samples are listed in Table I together with the thicknesses, t_I and t_S, and the glass transition temperatures, $T_{g,I}$ and $T_{g,S}$, of their PI and PS microdomains, respectively. Microdomain sizes were determined from SAXS patterns recorded at room temperature. All samples, except the viscous sample SI-5k ($M_n = 4.8 \times 10^3$) and the rubbery sample SI-8k ($M_n = 8.2 \times 10^3$), yielded patterns exhibiting a minimum of three equidistant reflections in agreement with lamellar packing. Some of these patterns are depicted in Figure 1. It may be seen that the even-ordered reflections are systematically weak (or absent) as expected for systems of alternating lamellae of close to 1:1 volume fraction.[12,13] Another feature of the SAXS patterns is the gradual extinction of the highest order reflections with decreasing molecular weight. This change may be interpreted in terms of paracrystalline distortion.[12] It indicates a progressive deterioration of the long-range order (or grain integrity) in the mesomorphic materials. On this ground, samples SI-5k and SI-8k, which exhibit a single reflection, may no longer be considered as ordered lamellar systems.

The microdomain thicknesses, t_I and t_S, quoted in Table I were computed by means of the following straightforward formulas

$$t_S = \varphi_S d \quad (1)$$

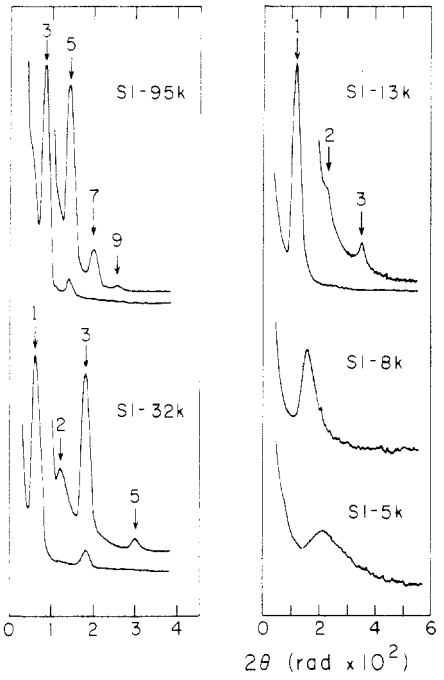

Figure 1. Small-angle X-ray scattering curves measured on the rigid samples SI-95k, SI-32k, and SI-13k, the rubbery sample SI-8k, and the viscous sample SI-5k. For the rigid samples, two curves are shown with different exposure times. Arrows indicate the diffraction line positions calculated for a lamellar structure on the basis of the most intense reflection in each pattern.

$$t_I = (1 - \varphi_S)d \qquad (2)$$

in which d is the lamellar periodicity and φ_S is the PS microphase volume fraction. The SAXS pattern of sample SI-380k exhibited a poor resolution that prevented an accurate determination of d. In the case of samples SI-5k and SI-8k, eqs 1 and 2 were tentatively applied by using the Bragg spacing of their single reflection. The volume fraction φ_S was computed from the weight composition w_S of the samples by assuming a density for each microphase identical with that of the corresponding homopolymer, that is, 1.053 g/cm^3 for homo-PS and 0.905 g/cm^3 for homo-PI.

In a previous SAXS study made on shear-oriented SI samples of the same composition and presumably the same PI block microstructure as the present samples, Hadziioannou and Skoulios[14] claimed that an abrupt transition from a well-organized lamellar morphology to a two-phase disordered structure occurs below a critical value of M_n located in the vicinity of 2×10^4. On the basis of the SAXS patterns recorded for the present specimens, there is no indication of such a sharp transition. Moreover, lamellar packing is still observed for a sample (SI-13k) having a molecular weight inferior to the quoted limit of 2×10^4. In view of this discrepancy, it was interesting to compare the molecular weight dependence of the lamellar spacings corresponding to the two sets of samples. Such a comparison is depicted in Figure 2 under the form of bilogarithmic plots of d as a function of M_n. Also included in these plots are the spacing data derived from the single reflection observed for the materials at the lower end of the molecular weight range. Though both sets of data are roughly superimposable, there is a marked difference concerning their respective analytical expression in terms of a power law of M_n. Indeed, a linear least-squares fit of the present data yields the relationship $d = 0.0205M_n^{0.69}$ (nm) while, as quoted by Hadziioannou and Skoulios,[14] a similar fit made on their data (for $M_n > 2 \times 10^4$) yields the relationship $d = 0.006M_n^{0.79}$ (nm). Note that the former

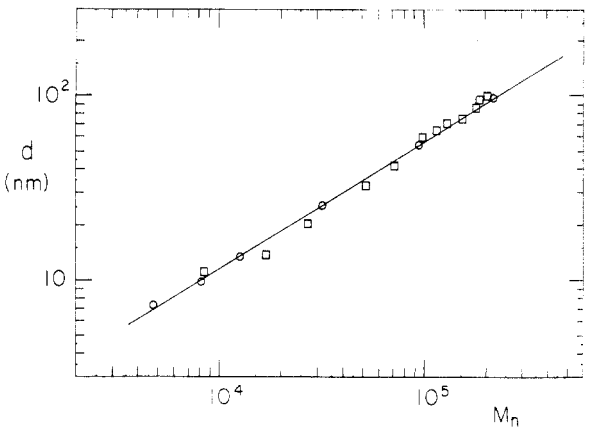

Figure 2. Bilogarithmic plot of the periodicity, d, determined by SAXS as a function of the SI block polymer molecular weight, M_n. A comparison is made of the present data (circles) with the data quoted by Hadziioannou and Skoulios[14] (squares) for shear-oriented specimens (see text).

is in better agreement with the power law $d \propto M^{0.64}$ predicted by Helfand and Wasserman on the basis of their narrow-interphase equilibrium theory for mesomorphic block polymers.[15] Also, it nearly coincides with the empirical relationship $d = 0.024M_n^{0.67}$ (nm) reported by Hashimoto et al.[13] for solvent-cast SI samples ($2 \times 10^4 \leq M_n \leq 1 \times 10^5$) comprising PI blocks having a high content (97%) of 1,2- and 3,4-vinyl units.

Many factors could account for the difference between our results and those of Hadziioannou and Skoulios.[14] Among them, there is the possibility in either study of having a systematic error related to molecular weight or Bragg spacing determination, or both. Another explanation is that shear-oriented specimens could exhibit some structural modifications with respect to solvent-cast specimens. An important result of the present SAXS study is that the periodicity in mesomorphic materials of very low molecular weight appears to vary with M_n according to the same power law as the lamellar spacings of the more ordered high molecular weight materials.

$T_{g,I}$ and $T_{g,S}$ values quoted in Table I correspond to the temperatures at half-height of the well-separated c_p jumps recorded upon the first heating of each specimen in the DSC apparatus. The data for samples SI-5k, SI-8k, and SI-13k, as well as their interpretation in terms of phase separation, were reported in an earlier work[10] dealing with the thermal behavior of low molecular weight SI samples. In Figure 3 a comparison is made of $T_{g,I}$ and $T_{g,S}$ with T_g data obtained for homo-PI and homo-PS, respectively, over the same molecular weight ($M_{n,I}$ and $M_{n,S}$) range as the PI and PS blocks in the SI samples. The main feature of this comparison is the occurrence of an important lowering of $T_{g,S}$ with respect to homo-PS for $M_{n,S}$ (or $M_{n,I}$) lower than ca. 2×10^4 and a concomitant but less important elevation of $T_{g,I}$ with respect to homo-PI. These changes occur at a global molecular weight M_n close to 4×10^4, that is, well above the limit where long-range lamellar packing disappears in the present set of samples. Also, both $T_{g,I}$ and $T_{g,S}$ exhibit a monotonous variation with M_n, a behavior that may reinforce our foregoing conclusion that there is no abrupt change of morphological structure at a critical value of M_n.

The more pronounced T_g change for the glassy microphase compared to the rubbery microphase is a general characteristic for PS-containing low molecular weight block polymers.[16-18] This feature has been quoted for materials comprising other rubbery microphases such as polybutadiene[16,17] and poly(dimethylsiloxane).[18] Different

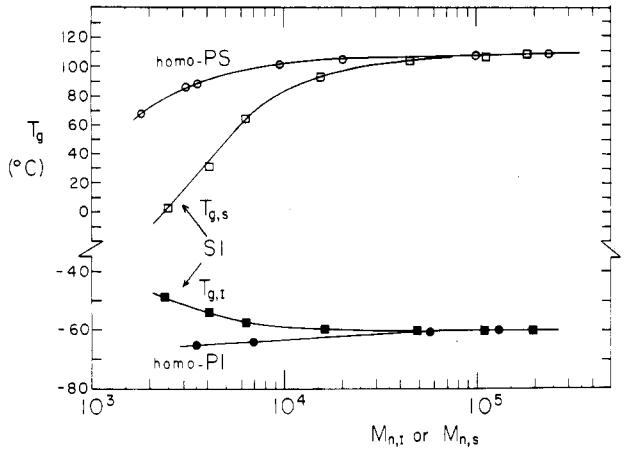

Figure 3. Comparison of $T_{g,I}$ and $T_{g,S}$ of the SI block polymers with T_g's of homo-PI and homo-PS having the same molecular weights ($M_{n,I}$ and $M_{n,S}$) as the PI blocks and the PS blocks, respectively. Measurements made by DSC at a heating rate of 40 °C/min.

interpretations have been proposed to explain this particular behavior. Kraus and Rollmann[16] suggested the possibility of an asymmetric mixing of the unlike components at the microdomain interface yielding an interphase layer rich in PS. According to this model,[16] with decreasing microdomain size, the volume fraction of the interphase layer would progressively increase to the detriment of the pure PS and PI microphases. The former would be the first to disappear owing to the asymmetric mixing.

In our earlier work[10] on low molecular weight SI materials, an alternative interpretation was given to the $T_{g,S}$ depression in terms of dynamical interactions taking place through the covalent bonds at the boundary of the unlike microphases. The standpoint for this interpretation was the measurement of a molecular weight independent value for the heat capacity increase, Δc_p, at $T_{g,I}$. Indeed, this quantity was almost identical with that of homo-PI when expressed per gram of PI in the SI samples. This ruled out the possibility of a partial mixing of the two components in the rubbery microphase. In turn, this suggested the presence of a pure PS microphase, albeit the values of Δc_p at $T_{g,S}$ were definitely lower than that of homo-PS. This latter feature was explained by postulating that the very onset of the PS microphase glass transition was probably occurring at a much lower temperature than the c_p jump observed on the DSC curves. In other words, the assumption was made that dynamical interactions at the microdomain boundary gave rise to an important spreading of the PS glass transition path toward the low-temperature region which could not be taken into account in the Δc_p determination. The existence of such a spreading was confirmed by Gaur and Wunderlich[19] on the basis of absolute c_p measurements made on high molecular weight polystyrene–poly(α-methylstyrene) di- and triblock polymers. Also observed by these authors was the inverse phenomenon, that is, a spreading toward the high-temperature region for the glass transition path of the softer microphase (PS in that case). In the case of the SI materials, this inverse effect is negligible, except for a very low molecular weight sample (M_n = 2.7 × 10^3)[10] not included in the present series.

NMR Evidence for Complete Microphase Separation in the SI Materials. The DSC data are not fully conclusive concerning the absence of any miscibility, particularly for the harder microphase in the low molecular weight materials. Thus, some of the solid samples have

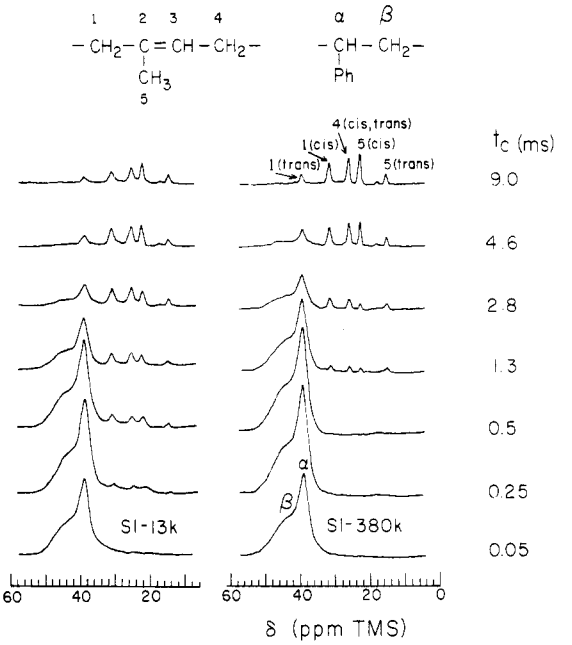

Figure 4. Aliphatic region of dipolar-decoupled CP-MAS solid-state ^{13}C NMR spectra (75.4 MHz) recorded at room temperature on samples SI-13k and SI-380k, respectively. Measurements made at various cross-polarization contact times, t_c, in the range 0.05–9 ms.

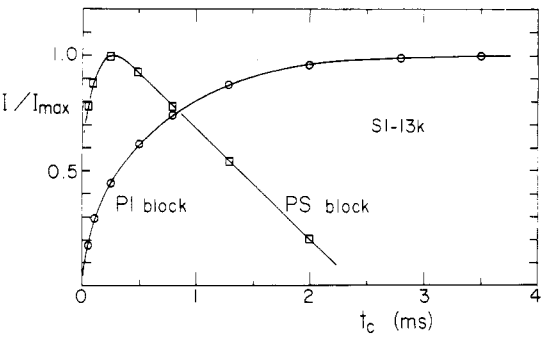

Figure 5. Plots as a function of cross-polarization contact time, t_c, of the relative intensities, I/I_{max}, of the PS and PI resonances, respectively, in CP-MAS ^{13}C NMR spectra of sample SI-13k (Figure 4). I_{max} corresponds to the maximum intensities observed at t_c = 0.25 and 4.6 ms for the PS and PI resonances, respectively.

been examined by ^{13}C NMR solid-state high-resolution spectroscopy. For this purpose, a series of measurements carried out under magic-angle spinning and proton dipolar decoupling have been made at various contact times, t_c, for cross-polarization (CP) transfer in the Hartmann–Hahn condition.[20] Figure 4 shows the results obtained at room temperature for samples SI-13k and SI-380k. In each case, buildup of the PS ^{13}C magnetization by CP transfer is maximum at t_c close to 0.25 ms. For this contact time, no PI resonance is perceptible in the spectrum of sample SI-380k, while small signals are present for sample SI-13k. In Figure 5, the relative intensities of the resonances of each component (PS and PI units) are plotted as a function of t_c for sample SI-13k. It may be seen that for $t_c < 0.25$ ms the magnetization of the PI units exhibits a uniform increase at a rate that is markedly lower than that of the PS units. This clearly indicates that one deals with components that belong to distinct phases. On the other hand, when compared on the basis of half-magnetization contact time, $t_{c,1/2}$, the rate of magnetization of the PI units in sample SI-13k was about one order of magnitude greater than that of sample SI-380k. This difference is remarkable, particularly if one considers that $T_{g,I}$ of sample SI-13k is only 2 °C above that of sample SI-380k. It is clear that

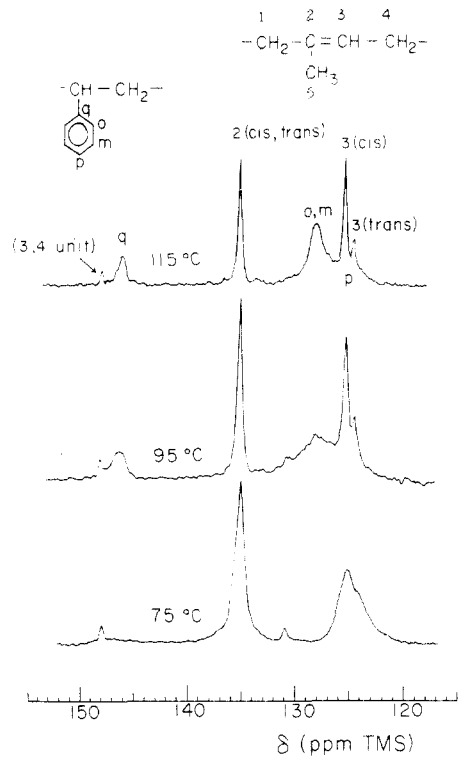

Figure 6. Aromatic-olefinic region of scalar-decoupled liquid-state ^{13}C NMR spectra (20.1 MHz) recorded on sample SI-5k at 75, 95, and 115 °C. Buildup of the PS resonances (125, 128, and 146 ppm) occurs near 85 °C.

the change in molecular motion responsible for this effect (CP transfer initial rate is an inverse function of molecular mobility[20]) concerns high-frequency motional modes that are not probed by the DSC technique.

The absence of styrene units in the rubbery microphase of the low molecular weight materials was confirmed by liquid-state ^{13}C NMR spectroscopy. Indeed, as illustrated in Figure 6 for sample SI-5k having the lowest molecular weight among the present samples, at 20.1 MHz no aromatic signal could be resolved in proton-decoupled spectra recorded at temperatures inferior to ($T_{g,S}$ + 80) °C, approximately. Above this limit, which roughly corresponds to 85 °C for sample SI-5k ($T_{g,S}$ = 3 °C) and 110 °C for sample SI-8k ($T_{g,S}$ = 31 °C), buildup of aromatic resonances occurs progressively, indicating the onset of high-frequency motion for the PS units. But even in the most favorable case, that is, for sample SI-5k at 115 °C (Figure 6), the PS resonances remain considerably broader than the PI resonances, indicating that each component is confined in a distinct microphase that exhibits its own dynamical behavior.

In a recent work by Gronski et al.,[21] solid-echo broadband ^2H NMR measurements have been reported on two SI block polymers of the same molecular weight and composition (M_n = 1 × 10^4, w_S = 0.50), each comprising a short chain of either deuterated PS (M_n = 4 × 10^3) or deuterated PI (M_n = 2 × 10^3) intercalated at the chemical junction between the unlike components. The relative intensity of the ^2H solid-echo resonance of each material exhibited a minimum at a temperature that could be correlated with either $T_{g,S}$ or $T_{g,I}$ measured by DSC. In agreement with the present T_g data, the former exhibited a depression of 43 °C with respect to deuterated homo-PS while the latter exhibited an elevation of 13 °C with respect to deuterated homo-PI. Another feature of the intensity curves as a function of temperature was a marked increase of dispersion width for the curve of the deuterated PS blocks compared to that of deuterated homo-PS. Although Gronski et al.[21] interpreted this behavior by first considering the possibility for an asymmetric mixing of the unlike components at the microdomain boundary, they noted that this interpretation was challenged by the line-width data. Indeed, at 25 °C the deuterated PI blocks yielded a narrow Lorentzian line while the deuterated PS blocks yielded about the same quadrupolar splitting as deuterated homo-PS, indicating that both components were confined in distinct regions of the system.

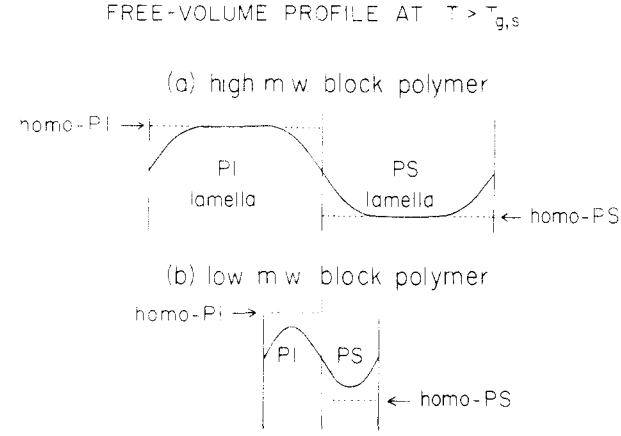

Figure 7. Free-volume model for PS microphase vitrification in SI lamellar block polymers. At $T > T_{g,S}$, both microphases are liquid-like and dynamical interactions at the microphase boundary yield a gradient of free volume near the interfaces. For high molecular weight SI samples (a), free volume in the core of the PS microdomains remains close to that of homo-PS. For low molecular weight samples (b), an elevation of free volume occurs in the core of the PS microdomains due to its closer distance from the interfaces. This change would explain the important lowering of $T_{g,S}$ with decreasing M_n below ca. 4 × 10^4.

Free-Volume Model for PS and PI Microphase Vitrification. The above evidences for complete phase separation in SI block polymers of low molecular weight reinforce our earlier proposal[10] that the marked lowering of $T_{g,S}$ with decreasing M_n might be due to dynamical interactions instead of an asymmetric mixing as proposed by Kraus and Rollmann.[16] In that respect, an interpretation based upon free-volume perturbation due to the chemical links at the microdomain boundary could also account for the asymmetric behavior of $T_{g,S}$ and $T_{g,I}$. This is true particularly if one considers that the vitrification of each microphase is expected to take place in very distinct physical conditions.

Upon cooling, vitrification of the PS lamellae occurs in a situation where both microphases are liquid-like. As depicted in Figure 7, at temperatures above $T_{g,S}$ the free-volume profile in the direction perpendicular to the lamellar interface should exhibit a periodic variation from one microphase to the other. This variation should reflect the difference in cohesive energy density of the pure components. Owing to the chemical links between the unlike components, the free-volume change at the boundary of the liquid microphases should not be sharp but spread over a layer of a finite thickness on either side of the interface. For high molecular weight materials (Figure 7a), the thickness of these interface layers would be small compared to the thickness of the lamellae. Then the polymer segments in the core of the lamellae would be in a region where free volume would be unchanged with respect to the corresponding homopolymer. But for molecular weights inferior to a critical size (Figure 7b), the interface layers on either side of a given lamella would overlap and the free

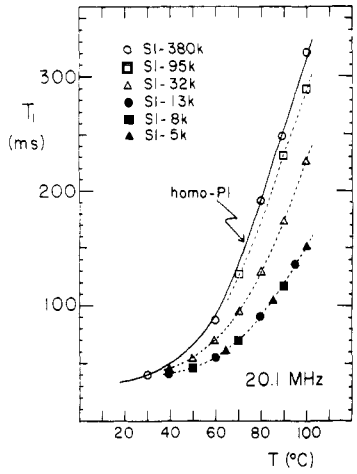

Figure 8. Temperature dependence of T_1 for the methylene C_1 resonance (20.1 MHz) of the PI cis-1,4 units in SI samples of different molecular weights. The full line corresponds to homo-PI data reported in the former work.[9]

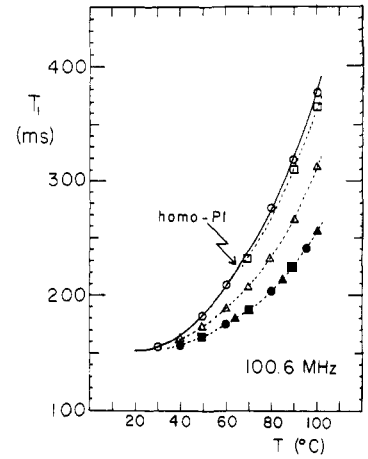

Figure 9. Temperature dependence of T_1 for the methylene C_1 resonance (100.6 MHz) of the PI cis-1,4 units in SI samples of different molecular weights. The full line corresponds to homo-PI data reported in the former work.[9] Same data point symbols as in Figure 8.

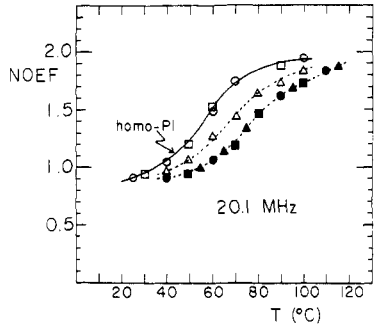

Figure 10. Temperature dependence of NOEF for the methylene C_1 resonance (20.1 MHz) of the PI cis-1,4 units in SI samples of different molecular weights. The full line corresponds to homo-PI data reported in the former work.[9] Same data point symbols as in Figure 8.

volume in the core of the lamellae would no longer be that of the corresponding homopolymer. In our earlier work,[10] it has been proposed that this effect accounts for both the $T_{g,S}$ depression and the lower value of Δc_p at $T_{g,S}$. According to this interpretation, the c_p jump recorded by DSC would correspond to the fraction of the PS segments located in the core of the lamellae, that is, in the region where both gradient of free volume and free volume are minimum. The glass transition for the PS segments near the interface, that is, in the region characterized by an important gradient of free volume, would be spread over a temperature range below the observed c_p jump. For this reason, it would be indistinguishable from the base-line drift on the DSC curves.

Contrary to the foregoing situation, vitrification of the interface layers in the PI lamellae should not be governed by dynamical interactions with the adjacent (PS) lamellae since segmental motion in the latter is already frozen at temperatures well above $T_{g,I}$. It would rather depend upon the free-volume perturbation (with respect to homo-PI) arising from the immobilization of the PI units covalently linked to the glassy microphase. Though such a perturbation would contribute to a premature vitrification of the PI interface layer, the latter would take place at a temperature that would depend upon the dynamics of the PI chains only. It is presumably for this reason that, contrary to the PS lamellae, the PI lamellae exhibit a sharp glass transition indicated by a Δc_p value at T_g that does not depart significantly from that of homo-PI. It is probably for the same reason that a T_g elevation with respect to homo-PI occurs only for samples of very low molecular weight in which a large fraction of the PI segments are located at a proximity from the microdomain interface.

T_1 and NOEF Study. T_1 data measured at 20.1 and 100.6 MHz for the methylene C_1 carbon in the cis-1,4 units of the PI blocks are plotted as a function of temperature in Figures 8 and 9, respectively. For each Larmor frequency, a master curve (full line) is drawn that depicts the temperature dependence of T_1 for homo-PI of the same microstructure as in the PI blocks of the SI samples. These curves correspond to molecular weight independent data obtained for two homo-PI samples with $M_n = 7 \times 10^3$ and 1.3×10^5, respectively.[9] Inspection of Figures 8 and 9 shows that no change of T_1 occurs with respect to the master curves in the case of sample SI-380k, having the highest molecular weight among the present samples. It may also be seen that with decreasing molecular weight (or microdomain thickness), T_1 remains unchanged down to ca. $M_n = 9.5 \times 10^4$ (sample SI-95k), after which it decreases abruptly toward an asymptotic value. This feature is indicated by the superimposition of the T_1 data obtained for the low molecular weight samples SI-13k, SI-8k, and SI-5k, respectively. Sample SI-32k of intermediate molecular weight exhibits T_1 values at about half the height between those of the high and low molecular weight samples.

A very similar behavior may be observed in Figure 10, where NOEF data measured at 20.1 MHz are plotted as a function of temperature. The data for samples SI-380k and SI-95k are nearly superimposable on the sigmoidal master curve drawn from the homo-PI data. Those for samples SI-13k, SI-8k, and SI-5k merge into a common sigmoidal curve shifted to higher temperatures with respect to the master curve, while those for sample SI-32k lie on an intermediate curve. The common feature of all these curves is a leveling off at a value close to 0.9 with decreasing temperature.

Analysis of T_1 and NOEF ^{13}C data in terms of segmental motion is not a simple matter. For proton-bearing carbons and under the assumption of a purely dipolar relaxation mechanism, both these quantities are governed by the spectral density function, $J(\omega)$, according to the well-known relationships[22]

$$T_1^{-1} = nA[3J(\omega_C) + J(\omega_H - \omega_C) + 6J(\omega_H + \omega_C)] \quad (3)$$

$$A = (\mu_0/4\pi)^2\hbar^2\gamma_C^2\gamma_H^2/10r^6 \quad (4)$$

$$\text{NOEF} = (\gamma_H/\gamma_C)\frac{6J(\omega_H + \omega_C) - J(\omega_H - \omega_C)}{3J(\omega_C) + J(\omega_H - \omega_C) + 6J(\omega_H + \omega_C)} \quad (5)$$

in which γ_C and γ_H are the magnetogyric ratios of the ^{13}C and ^1H nuclei, respectively, μ_0 is the vacuum magnetic permeability, $\hbar$ is Planck's constant, n is the number of directly bonded protons, and r is the C–H bond length. For $r = 0.109$ nm, the value generally quoted for an sp^3 group, the constant A is equal to 2.15×10^9 s^{-2}.

Physically, the function $J(\omega)$ characterizes the frequency distribution of the local magnetic fields produced by the motion of the ^1H nuclei at the proximity of the ^{13}C nuclei. In eq 3, the assumption is made that a predominant effect upon relaxation arises from the directly bonded protons. Therefore, prior to any interpretation of T_1 or NOEF data, one has to postulate an appropriate model for the C–H bond motion. For C–H bonds undergoing a rapid isotropic rotation characterized by a correlation time τ (the rigid-rotor model), $J(\omega)$ is given by the familiar expression[4]

$$J(\omega) = \tau/(1 + \omega^2\tau^2) \quad (6)$$

For C–H bonds located within the backbone of a flexible polymer chain, the main sources of high-frequency motion are small-amplitude oscillations (or partial rotations) and local conformational rearrangements. The combination of these fluctuations necessarily leads to a distribution of motional modes that depends upon the chemical structure of the polymer in addition to the temperature and other variables such as dilution and molecular segregation. Although a modeling of this distribution is possible by using a phenomenological approach, together with some simplifying assumptions,[4,5,9] more satisfying should be an interpretation based upon a physical model for chain dynamics. In this respect, several theories have been proposed on the very subject of conformational rearrangements in flexible polymer chains.[23] Among these theories, the most successful ones appear to be the three-bond jump model proposed many years ago by Jones and Stockmayer[24] and the more recent two-state model proposed by Hall and Helfand.[25] Either of these models leads to an expression for $J(\omega)$ that allows an interpretation of the relaxation data in terms of two distinct physical quantities. In the Jones–Stockmayer theory,[24] these quantities are the harmonic average correlation time for three-bond cooperative rearrangements and a discrete number that characterizes the segment length over which bond directional correlations exist. In the Hall–Helfand theory,[25] the two adjustable parameters are distinct correlation times. One corresponds to cooperative rearrangements involving first-neighbor bond pairs and the other corresponds to isolated single-bond rearrangements.

The merits of these two models have been thoroughly tested in a comparative study reported by Connolly et al.[26] In this study performed on diluted polycarbonates, either model provided a coherent interpretation of a number of ^{13}C and ^1H T_1 data, each measured at two Larmor frequencies and over a wide range of temperatures (−20 to +120 °C). Interestingly, the correlation times for cooperative motion inferred from both these models were nearly identical, exhibiting the same activation energy close to 20 kJ/mol. The one and only difference concerned the second parameter in each theory. The kinetic segment length parameter in the Jones–Stockmayer model was almost invariant over the entire range of temperatures, while the second correlation time in the Hall–Helfand model exhibited a temperature dependence very similar to that of the cooperative process. However, this second correlation time was by more than one order of magnitude longer than the former, indicating a predominance of the cooperative motion in the relaxation mechanism.[26]

Recent works dealing with bulk elastomers allowed the testing of these two models in more severe conditions, that is, in (or near) the temperature region where the T_1 magnitude exhibits a minimum.[6-9] Since this region is located only 40–50 °C above the range where complete loss of resolution occurs in conventional spectra recorded on elastomers, it corresponds to a situation in which important motional restrictions begin to appear in the materials. As in the study made on diluted polycarbonates, simultaneous fits of ^{13}C T_1 data measured at two Larmor frequencies were attempted over a range of temperatures by using either one of these models. The Hall–Helfand model was examined by Dejean de la Batie et al.[6-8] in a work dealing with a number of chemically different elastomers including bulk PI.[8] Note that these authors have proposed a modification to this model that will be discussed shortly. For each elastomer, they noted an important failure of the Hall–Helfand model in the temperature region near the T_1 minimum. In any case and for the two Larmor frequencies (25.1 and 62.5 MHz), the theoretical values of T_1 allowed by the model at the T_1 minima were considerably inferior to the experimental values. For instance, in the case of bulk PI for which the methylene T_1 minima are located near 20 °C, the magnitudes of the theoretical values were about half those of the experimental values at both fields.[8] The Jones–Stockmayer model was not examined by Dejean de la Batie et al. However, according to our parallel investigation made on bulk PI at 20.1 and 100.6 MHz,[9] this model also exhibits a failure near the T_1 minima. Although a simultaneous fit of the methylene T_1 data at both frequencies was possible down to ca. 40 °C, some discrepancies occurred below this temperature. For instance, the best fit at 20 °C was a compromise in which the theoretical curves were 30% above the 20.1-MHz data and 13% below the 100.6-MHz data, respectively.

In order to rationalize the failure of the Hall–Helfand model, Dejean de la Batie et al.[6] have suggested, after a proposition of Howarth,[27] that a fast libration of the C–H bonds may contribute to spin relaxation in addition to the conformational rearrangements. By first assuming, as in Woessner theory for internal rotation,[28] that this motion is independent of the conformational rearrangements and second that its correlation time, τ_L, is much shorter than those of the latter, they derived the following expression for $J(\omega)$:[6]

$$J(\omega) = (1 - a)\,\text{Re}\,[1/(\alpha + i\beta)^{1/2}] + a[\tau_L/(1 + \omega^2\tau_L^2)] \quad (7)$$

$$1 - a = [(\cos\theta - \cos^3\theta)/2(1 - \cos\theta)]^2 \quad (8)$$

$$\alpha = \tau_2^{-2} + 2\tau_1^{-1}\tau_2^{-1} - \omega^2 \quad (9)$$

$$\beta = -2\omega(\tau_1^{-1} + \tau_2^{-1}) \quad (10)$$

The term proportional to the factor $(1 - a)$ in eq 7 corresponds to the $J(\omega)$ function that may be derived from the Hall–Helfand model.[6] Its composite variables α and β contain the correlation times τ_1 and τ_2 corresponding to the cooperative and the single-bond rearrangements, respectively. The angle θ, which the factor $(1 - a)$ depends upon, corresponds to the libration angular amplitude of the C–H bonds. Also note that Dejean de la Batie et al.[6] have suggested an alternative interpretation to the Hall–Helfand correlation time τ_2 in terms of a damping factor

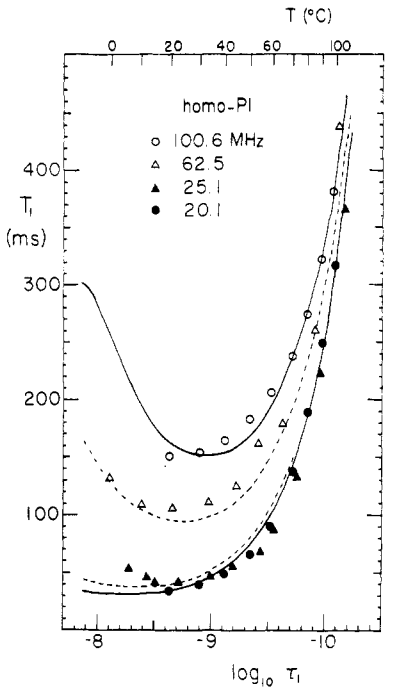

Figure 11. Fit of the new model proposed by Dejean de la Batie et al.[6] to the homo-PI 20.1- and 100.6-MHz T_1 data. Theoretical curves (full and dashed curves) of T_1 as a function of log τ_1 were computed according to eq 7 with $a = 0.4$, $\tau_1/\tau_L = 150$, and $\tau_2/\tau_1 = 5$. Ratio τ_2/τ_1 was adjusted in the temperature range 70–100 °C, while parameter a and ratio τ_1/τ_L were adjusted in the temperature range 20–60 °C. It may be seen that this fit provides good prediction of the 25.1- and 62.5-MHz data quoted in ref 8 for a homo-PI sample having a greater cis-1,4 unit content (92%) than the present samples (71%).

for cooperative motion. According to this interpretation, the magnitude of τ_2 should increase with increasing segment length for bond directional correlation.

T_1 Modeling. As shown in Figure 11, eq 7 may be easily adjusted to coarsely fit the 20.1- and 100.6-MHz T_1 data corresponding to the master curves in Figures 8 and 9, respectively. For that purpose, the temperature scale (upper scale) of each pair of T_1 data (20.1 and 100.6 MHz) was positioned in order to obtain the best fit with the corresponding theoretical curves of T_1 as a function of log τ_1. As in the work by Dejean de la Batie et al.,[6-8] these curves (full curves) were computed by using temperature-independent values for the parameter a and the ratios τ_1/τ_L and τ_2/τ_1 of the three distinct correlation times in the new model. The best values of these parameters ($a = 0.4$, $\tau_1/\tau_L = 150$, and $\tau_2/\tau_1 = 5$) were preadjusted on a trial and error basis by focusing on either the low-temperature range (for a and τ_1/τ_L) or the high-temperature range (for τ_2/τ_1) of the data.

Also shown in Figure 11 are plots as a function of the temperature (upper scale) of the 25.1- and 62.5-MHz T_1 data reported by Dejean de la Batie et al.[8] for the same ^{13}C nuclei in a homo-PI sample having a greater cis-1,4 unit content (92%) than the present samples (71%). It may be seen that these data also exhibit a coarse agreement with the corresponding theoretical curves (dashed curves) computed on the basis of the foregoing parameters. Note that among these parameters, only the magnitude of the ratio τ_2/τ_1 differs from that ($\tau_2/\tau_1 = 40$) quoted by Dejean de la Batie et al.[8] This difference is essentially due to a discrepancy concerning the 100.6-MHz data. Indeed, when the values of τ_1 deduced from the fit reported by these authors (Figure 4 in ref 8) are used for predicting the values of T_1 at this Larmor frequency, the latter are systematically greater than the experimental values. The

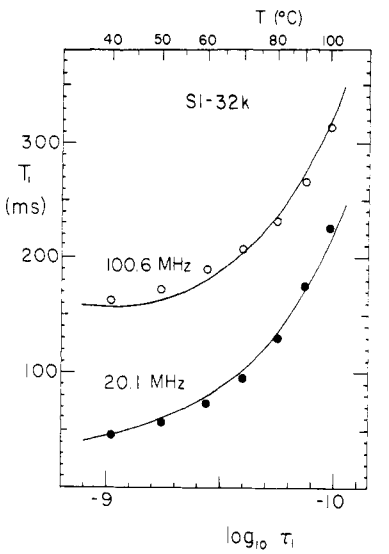

Figure 12. Fit of the new model proposed by Dejean de la Batie et al.[6] to the 20.1- and 100.6-MHz T_1 data of sample SI-32k. Theoretical curves of T_1 as a function of log τ_1 were computed according to eq 7 with $a = 0.4$, $\tau_1/\tau_L = 150$, and $\tau_2/\tau_1 = 7$. Same fitting procedure as in Figure 11.

discrepancy is notably important in the upper range of temperatures where computed values of T_1 are the most sensitive to the ratio τ_2/τ_1. Its magnitude increases from 10% at 60 °C to 25% at 100 °C. In this range of temperatures, the present fit (Figure 11) exhibits an acceptable agreement with all the experimental data, including those of Dejean de la Batie et al. The discrepancy observed below ca. 60 °C in the present fit is partly due to a variation of τ_2/τ_1 with temperature. This point will be discussed shortly. Another point concerns the ratio τ_1/τ_L. As reported by Dejean de la Batie et al.,[8] the magnitude of this ratio cannot be determined with accuracy. Its value of 150 is a lower limit below which fitting discrepancy occurs in the region of the T_1 minima. Greater values of this parameter (for instance 500) would yield a minor change in the theoretical curves depicted in Figure 11.

The fit in Figure 11 for homo-PI equally applies to the T_1 data of sample SI-380k. Similar fits made with the T_1 data of samples SI-32k and the composite data of samples SI-13k, SI-8k, and SI-5k are shown in Figures 12 and 13, respectively. These fits were obtained by adjusting the parameter a and the ratio τ_1/τ_L to the same values as for homo-PI. However, they required slight changes to the ratio τ_2/τ_1, that is, a value of 7 for data of sample SI-32k and a value of 10 for the composite data of the low molecular weight SI materials. Since the magnitude of τ_2/τ_1 appears to be correlated with that of the T_1 range in each set of data, attempts were made to adjust this ratio as a function of the temperature. It turned out that the same value of this ratio, namely, $\tau_2/\tau_1 = 10$, gave a good fit to the three sets of data in the temperature range below 60 °C. Such a fit is depicted in Figure 14 for homo-PI. A comparison of this fit with the former fit (Figure 11) clearly indicates that τ_2/τ_1 decreases with increasing temperature. However, the temperature dependence of τ_2/τ_1, like that of T_1, appears to be considerably attenuated with decreasing lamella thickness.

Figure 15 shows Arrhenius plots of the correlation times τ_1 deduced from the three fits depicted in Figures 11–13, respectively. In the case of homo-PI (or sample SI-380k), a plot is also made (dashed curve) of the τ_1 data deduced from the second fit depicted in Figure 14. This alternative plot is limited to a temperature range below 60 °C. The Arrhenius plots in Figure 15 exhibit the same

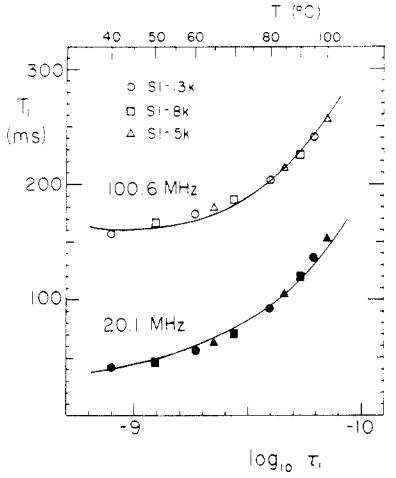

Figure 13. Fit of the new model proposed by Dejean de la Batie et al.[6] to the 20.1- and 100.6-MHz T_1 composite data of samples SI-13k, SI-8k, and SI-5k. Theoretical curves of T_1 as a function of log τ_1 were computed according to eq 7 with $a = 0.4$, $\tau_1/\tau_L = 150$, and $\tau_2/\tau_1 = 10$. Same fitting procedure as in Figure 11.

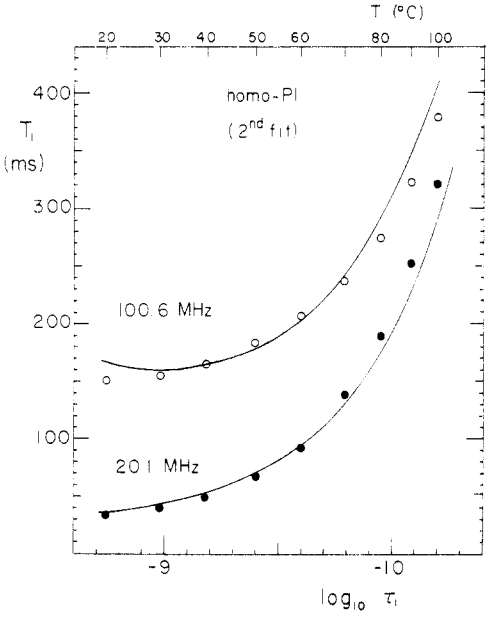

Figure 14. Second fit of the model proposed by Dejean de la Batie et al.[6] to the homo-PI T_1 data. Theoretical curves of T_1 as a function of log τ_1 were computed according to eq 7 with $a = 0.4$, $\tau_1/\tau_L = 150$, and $\tau_2/\tau_1 = 10$. Same fitting procedure as in Figure 11 except that the ratio τ_2/τ_1 was adjusted in the temperature range 20–60 °C instead of 70–100 °C.

type of singularity as that reported in our former analysis of the homo-PI data by means of two other models, namely, the Jones–Stockmayer model and the log χ^2 rigid-rotor distribution model.[9] This singularity is a change of regime indicated by the presence of two segments of different slope in each plot. With decreasing lamellar thickness in the block polymers, the point of intersection of these segments is shifted to higher temperatures. It is located near 63 °C (dashed curve) for homo-PI (or sample SI-380k), near 75 °C for sample SI-32k, and near 79 °C for the low molecular weight SI materials. This change is concomitant with an increase of τ_1 with decreasing lamellar thickness at a given temperature. However, as indicated by the same values of T_1 (or τ_1) for samples SI-13k, SI-8k, and SI-5k, both these effects exhibit an asymptotic behavior in the limit of a very small thickness.

In our former analysis of the homo-PI data,[9] a similar transition was observed near 66 °C in the Arrhenius plot of the harmonic average correlation time, τ_h, inferred from

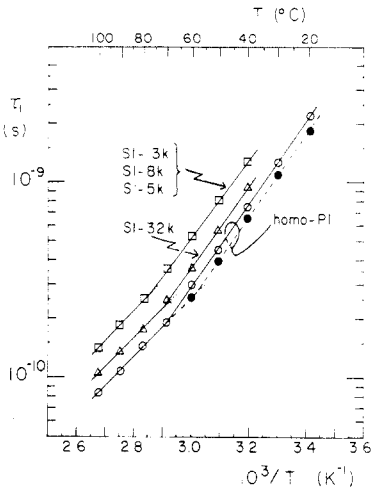

Figure 15. Arrhenius plots of the correlation times τ_1 for cooperative motion deduced from the fits shown in Figures 11–14. In each case, values of τ_1 were read at 10 °C intervals on the corresponding fit. For homo-PI, the full curve corresponds to the $\tau_2/\tau_1 = 5$ fit depicted in Figure 11, while the dashed curve corresponds to the $\tau_2/\tau_1 = 10$ fit depicted in Figure 14.

the Jones–Stockmayer model. A similar transition was also observed near 59 °C in the Arrhenius plot of the logarithmic average correlation time, τ_0, inferred from the log χ^2 distribution model. In the temperature range 40–100 °C, where the former model could perfectly fit the T_1 data, the magnitude of τ_0 was about twice as large as that of τ_h. The second adjustable parameter in these models, that is, the segment length for bond directional correlation in the former and the distribution width in the latter, each exhibited a sigmoidal increase with decreasing temperature.[9] This change was centered on the break in the corresponding Arrhenius plot. It provided evidence that the change in activation energy observed near 60 °C for τ_h (or τ_0) was associated with a change in motional cooperativity (or motional dispersion). At temperatures above 60 °C, the apparent activation energies, E_a, related to τ_h (15 kJ/mol) and τ_0 (19 kJ/mol) were comparable to those in the range 17–22 kJ/mol reported in similar studies made on a variety of diluted polymer systems.[26,29,30]

In the temperature range 20–100 °C, the magnitude of τ_1 for homo-PI is greater than that of τ_0 by a factor in the range 1.1–2.5. This difference is rather small if one considers that these quantities were inferred from very distinct models. However, a discrepancy occurs concerning the magnitudes of E_a deduced from the slopes of the low- and high-temperature segments in the Arrhenius plot of τ_1. Above 60 °C, E_a for τ_1 (29 kJ/mol) is markedly greater than the values (15 and 19 kJ/mol) reported for τ_h and τ_0.[9] In contrast, below 60 °C, E_a for τ_1 (41 kJ/mol) is inferior to the values (47 and 65 kJ/mol) reported for τ_h and τ_0.[9] These differences suggest the presence of some modeling background in either the present or the former analysis. The crucial point, however, is that the three distinct models yield the same overall feature concerning segmental motion in homo-PI: that is, a clear evidence for a motional change at a temperature near (T_g + 120) °C. As shown later in this paper, this behavior is not specific to homo-PI. It also applies to the other elastomers studied by Dejean de la Batie et al.[6-8]

In a recent paper by Veissier et al.,[31] the dynamics of an anthracene-labeled homo-PI mixed with the same homo-PI as that studied by Dejean de la Batie et al.[8] was examined by means of fluorescence anisotropy decay measurements. Data are reported on the temperature dependence of τ_1 deduced from these measurements on

the basis of the Hall–Helfand model[25] and another model derived by Viovy et al.[23] Interestingly, Arrhenius plots of these data exhibit a change of slope near 50 °C very similar to that in Figure 15. Note that neither Dejean de la Batie et al.[8] nor Veissier et al.[31] reported this feature concerning τ_1. They rather made their analysis of τ_1 in terms of a linear form of the WLF equation,[32] and only Veissier et al.[31] reported a plot that included the data points. In this plot, as well as in a similar plot (not shown) of the present data, the data points exhibited evidence for a change of slope near 50–60 °C. This change, however, was less pronounced than that in the corresponding Arrhenius plots. In a paper by Törmälä,[33] a frequency–temperature relaxation map was compiled for natural rubber that may help to clarify this point. This map, which includes dielectric, mechanical, NMR, and ESR (spin probe) composite data, defines two distinct relaxation processes related to backbone motion in bulk homo-PI. One of these processes is related to the cooperative motion associated with T_g. It conforms to the WLF equation. The other process is related to a local backbone motion of higher frequency. It exhibits an Arrhenius behavior (E_a = 22 kJ/mol) over a wide range of temperatures that extends well below T_g. At temperatures greater than ca. 20 °C, these two relaxation processes merge and the resulting master curve departs from the WLF behavior. Though the merging point is not accurately defined in the map due to the scattering of the composite data, it is clear that, with increasing temperature well above T_g, cooperative motion progressively disappears in the material in favor of more local motional processes. It is thought that the break observed in the Arrhenius curves of τ_1 corresponds to this transition. Note that over the range of temperatures covered by the present study the methyl rotation in homo-PI remains well separated from the backbone motion. As reported in the former work on homo-PI,[9] its frequency at 100 °C is 2 orders of magnitude greater than that of the conformational jumps.

According to Dejean de la Batie et al.,[6-8] any change in motional cooperativity with increasing temperature should be quantified by a corresponding change in the ratio τ_2/τ_1. On the basis of the foregoing fits for homo-PI, this ratio exhibits a twofold decrease with increasing temperature in the range 40–100 °C. Though this result agrees with the conclusion inferred from the log χ^2 and Jones–Stockmayer models,[9] the exact physical meaning of the correlation time τ_2 in the new model remains to be confirmed. Indeed, in the Hall–Helfand theory,[25] this parameter is assumed to be related to isolated single-bond rearrangements, not to damping of motional diffusion. However, the fact that its magnitude is greater than that of τ_1 seems to rule out the possibility that this parameter could reflect the local motion identified in the relaxation map of natural rubber.

In view of this ambiguity concerning the new model, a second analysis of the block polymer T_1 data has been performed on the basis of a log χ^2 distribution of rigid rotors. According to Schaefer,[4] this distribution function, $F(S)$, is written in terms of a variable S, which is a b-base logarithmic function of τ

$$F(S) = (1/\Gamma(p))(pS)^{p-1}p \exp(-pS) \quad (11)$$

$$S = \log_b [1 + (b-1)(\tau/\tau_0)] \quad (12)$$

where τ_0 is the average correlation time corresponding to the mean value of S ($\bar{S} = 1$), p is a width parameter whose inverse corresponds to the variance, σ^2, of the distribution, and $\Gamma(p)$ is the Gamma function of p.

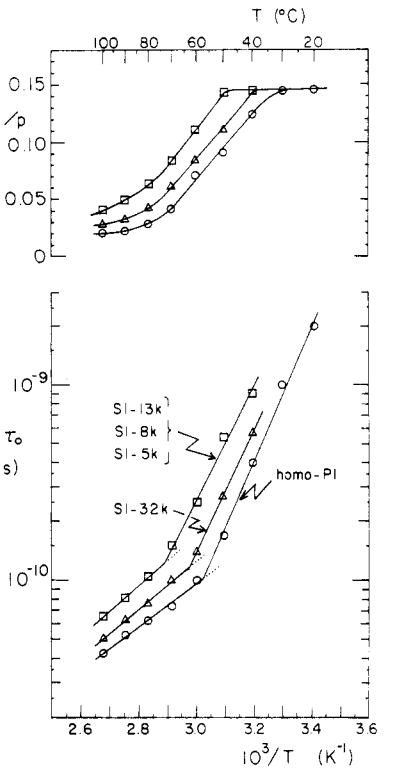

Figure 16. Arrhenius plots of the average correlation times τ_0 deduced from log χ^2 distribution modeling. Fits of eq 11 (with b = 1000) were applied at 10 °C intervals on the smooth curves drawn through the 20.1- and 100.6-MHz T_1 data depicted in Figures 8 and 9, respectively. Also shown for each system is the temperature dependence of the variance, $1/p$, of the log χ^2 distribution.

Under the assumption of a simple superposition of independent rigid rotors, the corresponding spectral density function $J(\omega)$ is obtained by averaging eq 6 over all values of S by means of $F(S)$. This average may be computed by numerical integration according to the following expressions:

$$J(\omega) = \int_0^\infty [\tau/(1 + \omega^2\tau^2)]G(\tau)\, d\tau \quad (13)$$

$$G(\tau)\, d\tau = F(S)\, dS \quad (14)$$

Equation 11 was modeled at intervals of 10 °C on the smooth curves drawn through the 20.1- and 100.6-MHz T_1 data of Figures 8 and 9, respectively. For that purpose, use was made of a logarithmic base of 1000 in eq 12 and the parameters τ_0 and p were adjusted in order to get computed values of T_1 at both fields with better than 2% agreement with the experimental values. The results of these fits are summarized in Figure 16 in which, for each system, an Arrhenius plot of τ_0 is presented together with the temperature dependence of the distribution width $1/p$. It may be seen that the effect of lamellar thickness upon τ_0 is nearly identical with that observed in Figure 15 for τ_1. The break in each Arrhenius curve is centered on the corresponding sigmoidal curve of $1/p$, the latter being shifted to higher temperatures with decreasing lamellar thickness. With respect to homo-PI (or sample SI-380k), the shift is ca. 6 °C for sample SI-32k and ca. 15 °C for the low molecular weight samples SI-13k, SI-8k, and SI-5k.

NOEF Predictions. From the log χ^2 distribution parameters τ_0 and $1/p$ deduced for each system, theoretical values of NOEF at 20.1 MHz were computed that all exhibited better than 10% agreement with the corresponding experimental data in Figure 10. As shown in

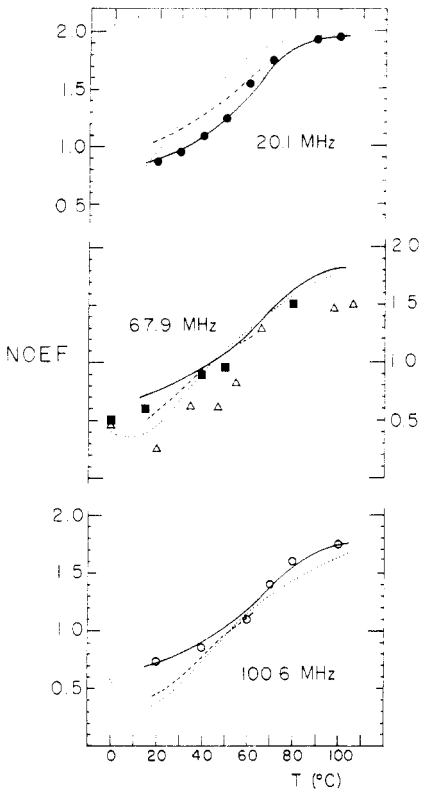

Figure 17. Temperature dependence of NOEF for homo-PI at various Larmor frequencies in the range 20.1–100.6 MHz. Included are 67.9-MHz data reported by Dekmezian et al.,[5] 62.5-MHz data (triangles) reported by Dejean de la Batie et al.,[8] and the data (20.1 and 100.6 MHz) reported in the former work.[9] Full curves depict the values predicted by means of the log χ^2 distribution model, with the parameters τ_0 and $1/p$ given in Figure 16. The other curves depict the values predicted by means of the model proposed by Dejean de la Batie et al.[6] Dotted curves correspond to the fit shown in Figure 11 with $\tau_2/\tau_1 = 5$. Dashed curves (in the range 20–60 °C) correspond to the fit shown in Figure 14 with $\tau_2/\tau_1 = 10$.

our former work on homo-PI,[9] such quantitative predictions for NOEF are results of primary importance. They confirm that the change of regime observed in the Arrhenius curves of τ_0 is not a modeling artifact. In addition, particularly instructive is the NOEF leveling off at a value close to 0.9 in the low-temperature range of the 20.1-MHz curves depicted in Figure 10. Indeed, this leveling off conforms to a limit behavior that may be theoretically predicted for an excessive dispersion of rigid rotors.[9] In that respect, the NOEF data in Figure 10 are in complete agreement with the temperature dependence of the distribution width $1/p$ inferred from the T_1 data.

Compared to the log χ^2 distribution model, the new physical model proposed by Dejean de la Batie et al. yielded less satisfying NOEF predictions. Indeed, over the range of temperatures inferior to ca. 50 °C for homo-PI and 80 °C for the other systems, all the predicted values were ca. 20–30% superior to the experimental data. In order to scrutinize the origin of this discrepancy, NOEF predictions made with both models were confronted with homo-PI data measured at various Larmor frequencies in the range 20.1–100.6 MHz. These data included 62.5- and 67.9-MHz data reported by Dejean de la Batie et al.[8] and Dekmezian et al.,[5] respectively, in addition to 20.1- and 100.6-MHz data measured in our laboratory.[9] As shown in Figure 17, the predictions made with the log χ^2 distribution model (full curves) exhibit an acceptable agreement with all the data except the 62.5-MHz data quoted by Dejean de la Batie et al.[8] In order to examine the effect of the ratio τ_2/τ_1 in the new model, two distinct series of curves were computed with this model. One series (dotted curves) is based upon the $\tau_2/\tau_1 = 5$ T_1 fit depicted in Figure 11, while the other (dashed curves) corresponds to the $\tau_2/\tau_1 = 10$ T_1 fit depicted in Figure 14. Inspection of these curves shows that the latter exhibit a better agreement than the former in the temperature range below 60 °C. This result is entirely consistent with the expectation based upon the T_1 fits. However, a discrepancy remains in this range of temperatures that could not be attenuated without changing the magnitude of the other parameters in the model. Thus, it is clear that the crucial problem encountered with the new model is the difficulty to properly adjust its numerous parameters.

Features of the Motional Perturbation Probed by T_1 and NOEF. A first feature of the motional perturbation in the PI lamellae is its localization within a region of finite thickness near the microdomain boundary. An indication of this feature is provided by the asymptotic behaviors of T_1 and NOEF at both extremes of the molecular weight (or lamellar thickness) range. A rough estimate of the thickness of the perturbed zone may be made by postulating that the T_1 data of samples SI-95k and SI-32k in the intermediate range correspond to a two-component volume-weighted average of these two asymptotic behaviors. In this hypothetical model, the assumption is made that one of the components, a high-T_1 component, behaves like homo-PI, while the other component, a low-T_1 component, behaves like the low molecular weight SI samples. The volume fractions of the low-T_1 component deduced from this model are 0.16 for sample SI-95k and 0.52 for sample SI-32k. When these fractions are applied to the half-thicknesses of the PI lamellae in these samples, they yield values of 2.4 and 3.6 nm, respectively, indicating an increase in the thickness of the perturbed zone with decreasing lamellar thickness. These results are consistent with the observation of a low-T_1 component behavior for the full thickness of the PI lamellae in sample SI-13k. Indeed, the half-thickness of the PI lamellae in this sample (3.6 nm) is identical with the thickness of the perturbed zone in sample SI-32k. Note that the foregoing estimations for samples SI-95k and SI-32k were made by assuming that the linear fits applied to the inversion–recovery data yielded T_1 values corresponding to the average values of the low- and high-T_1 components. In fact, it may be shown that such linear fits should provide good approximations of these average values for two-component (single-resonance) systems, like the present ones, in which the T_1 magnitudes of the individual components do not differ by a factor greater than 2.

A second feature of the motional perturbation probed by T_1 and NOEF is its similarity with that produced by an increase of chain stiffness in chemically different elastomers. Indeed, as shown in Figure 18, when log χ^2 distribution modeling is made on the methylene T_1 data reported by Dejean de la Batie et al.[6-8] for a series of four distinct elastomers with T_g values ranging from −110 to −26 °C, Arrhenius curves of τ_0 are obtained that exhibit a change of regime at a temperature corresponding to (T_g + 120) ± 10 °C. Though the high-temperature segments of all these curves exhibit the same apparent activation energy close to 19 kJ/mol, they are shifted upward with increasing T_g. Also depicted in Figure 18 is the temperature dependence of the distribution width, $1/p$, for each elastomer. The latter exhibits a sigmoidal variation centered on the temperature where a change of regime occurs in the corresponding Arrhenius plot. This general behavior indicates that at temperatures above the change

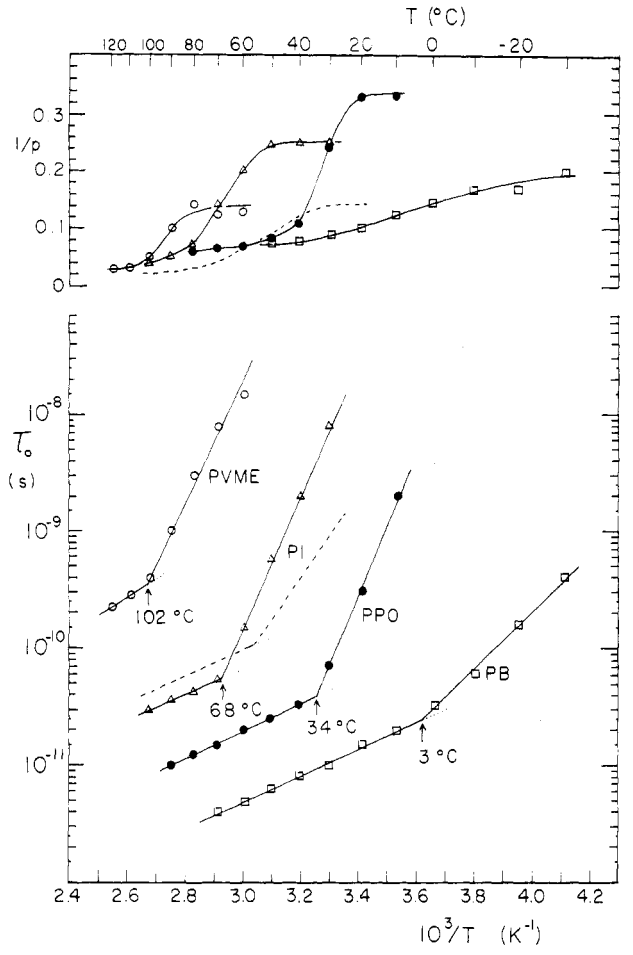

Figure 18. Arrhenius plots of the average correlation times τ_0 deduced from log χ^2 distribution modeling applied to the methylene T_1 data (25.1 and 62.5 MHz) reported by Dejean de la Batie et al.[6-8] for various elastomers. Plots are shown for poly(vinyl methyl ether) (PVME, T_g = −26 °C),[6] polyisoprene (PI, T_g = −60 °C),[8] poly(propylene oxide) (PPO, T_g = −75 °C),[7] and polybutadiene (PB, T_g, = −110 °C).[8] The present data for homo-PI are depicted by the dashed curve. Also shown for each elastomer is the temperature dependence of the variance, $1/p$, of the log χ^2 distribution.

of regime, the upper range of the motional spectrum in each elastomer (that is, the range probed by T_1) is dominated by a narrow distribution of conformational jumps involving about the same apparent internal barrier. The difference, however, is an average correlation time for these conformational jumps that, like T_g, appears to be modulated by the overall mobility of the chain backbones in the bulk material.

On the basis of this general behavior for homopolymers, the displacements observed in the Arrhenius curves of τ_1 and τ_0 for the low molecular weight SI materials would correspond to a T_g increase of ca. 15 °C. Though this prediction is in rough agreement with the $T_{g,I}$ elevations depicted in Figure 3 (6 °C for sample SI-13k, 11 °C for sample SI-8k, and 16 °C for sample SI-5k), the latter do not exhibit an asymptotic behavior as τ_1 and τ_0. This difference may be explained by considering that two distinct physical constraints result from the chemical junctions to the PS microphase. One of these constraints is the immobilization of the PI chain ends. The other is the increase in PI segment density near the microdomain boundary. According to the foregoing data concerning the $T_{g,I}$ elevations, it may be deduced that segment density increases gradually within the perturbed zone of 3.6 nm defined on the basis of the T_1 data. Therefore, the dominant factor upon T_1 and NOEF is not the change in segment density (or free volume) but the constraint resulting from the immobilization of the PI chain ends. A clear evidence of this feature is the apparent negligible effect of the PS microphase rigidity upon the magnitude of T_1 and NOEF. Indeed, over the temperature range 40–100 °C, the data of sample SI-5k, having a $T_{g,S}$ of 3 °C only, are entirely superimposable on those of sample SI-13k, having a $T_{g,S}$ of 65 °C.

A similar effect due to chain end immobilization was reported may years ago by Heatley and Begum[34] in a comparative study made on 5% solutions of a SBS (B = polybutadiene) block polymer in various solvents, including selective solvents for either the PB or the PS blocks. In dimethoxyethane, a nonsolvent for homo-PS, a marked decrease of both T_1 and NOEF was observed with respect to homo-PB, indicating an important perturbation of the high-frequency motion due to the presence of collapsed PS coils at the PB chain ends.

Interestingly, a similar effect was also reported by Dejean de la Batie et al.[7] for poly(ethylene oxide) (PEO) chains in amorphous polyurethane networks prepared with poly(ethylene glycol) (PEG) of different molecular weights in the range 400–1500. By using a separation procedure based upon a two-component model for T_1 (high- and low-T_1 components), they showed that a marked decrease of mobility occurred in the PEO chains with decreasing distance from the urethane junctions. This perturbation of the high-frequency motion in the PEO networks was explained by postulating that the urethane junctions interrupted the orientation diffusion processes along the chains. The argument for this interpretation was that the magnitude of τ_2/τ_1 deduced from the T_1 data was smaller for the networks prepared with PEG of M_n = 400, 600, and 1000 (τ_2/τ_1 = 30) than for the network prepared with PEG of M_n = 1500 (τ_2/τ_1 = 100). Unfortunately, it was overlooked that the actual magnitude of the very parameter τ_2 for motional cooperativity increased with decreasing PEO chain length. Indeed, with decreasing M_n of the network chains in the range 1500–400, τ_1 increased by more than 1 order of magnitude, indicating a threefold increase in τ_2. Therefore, the correct trend concerning orientation diffusion along the chains is just the opposite to that claimed by these authors. In other words, their data suggest an increase (not a decrease) in motional cooperativity with decreasing distance from the chemical junctions in the networks.

According to the present data, the same effect occurs with decreasing distance from the boundary in the SI samples. An explanation for this behavior is that chain end immobilization would considerably reduce the number of overall conformations capable of promoting independent local jumps along the chain backbones. This effect is similar to that resulting from an increase of chain stiffness in bulk homopolymers. Indeed, in this latter case, independent local jumps occur in significant amount only once the overall mobility of the chains reaches a certain level with increasing temperature. The temperature threshold for this behavior appears to roughly correlate with the quantity (T_g + 120) °C.

Line-Width Variation with Lamellar Thickness. Contrary to T_1 and NOEF, ^{13}C NMR line widths exhibit great sensitivity to the rigidity of the PS microphase. This effect is depicted in Figure 19, where line width at half-height, $W_{1/2}$, of the cis-1,4 unit methyl resonance measured at 20.1 MHz is plotted as a function of M_n for different temperatures in the range 40–90 °C. Similar plots (not shown) were obtained for the other resonances of the PI units. At 90 °C, that is, well above $T_{g,S}$ for the low mole-

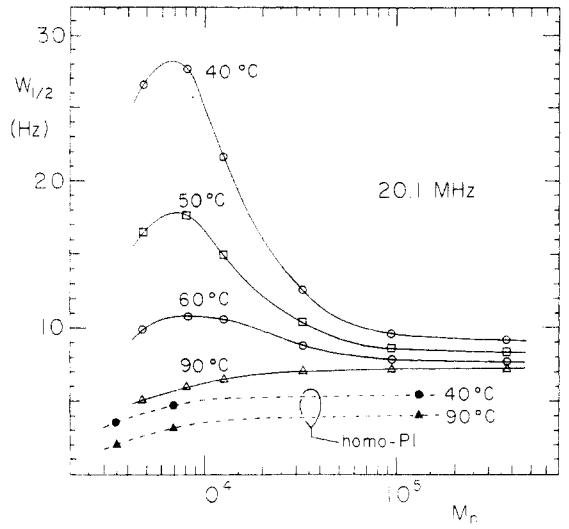

Figure 19. Plots as a function of M_n of line width at half-height, $W_{1/2}$, of the cis-1,4 unit methyl resonance for the SI and homo-PI samples. Measurements made on scalar-decoupled liquid-state ^{13}C NMR spectra (20.1 MHz) recorded at different temperatures in the range 40–90 °C with the same instrumental adjustments.

cular weight SI samples, $W_{1/2}$ exhibits a slight increase with M_n similar to that observed for homo-PI. At this temperature, $W_{1/2}$ of the block polymers is ca. 3 Hz larger than that of homo-PI. However, in the range 40–60 °C, each curve exhibits a maximum near $M_n = 7 \times 10^3$ where the magnitude of $W_{1/2}$ departs considerably from that of homo-PI. Furthermore, the amplitude of this maximum increases markedly with decreasing temperature. This indicates that a motional perturbation not probed by T_1 and NOEF occurs with increasing segment density in the PS microphase. As indicated by the convergence of each curve for M_n greater than ca. 9.5×10^4, this perturbation is also limited to PI segments located within a region of finite thickness near the microdomain boundary. By taking into account the variation of $T_{g,S}$ with decreasing M_n, it is clear that this perturbation becomes more and more accentuated with decreasing distance from the boundary. In fact, it is because $T_{g,S}$ decreases with decreasing M_n that a maximum is observed in the $W_{1/2}$ curves.[10]

The change in molecular motion associated with the vitrification of the PS microphase appears to concern the large-amplitude rearrangements in the lower range of the motional spectrum of the PI chains. This change presumably results from the free-volume depletion at the proximity of the glassy microdomains. Restriction of the large-amplitude segmental motion would produce chemical shift anisotropy or residual dipolar couplings (or both). This interpretation, which is consistent with the $T_{g,I}$ elevation for $M_n < 4 \times 10^4$ (Figure 3), is corroborated by the marked increase of the PI cross-polarization transfer rate at $T < T_{g,S}$ (Figure 4) for sample SI-13k with respect to sample SI-380k.

On this ground, it is clear that T_1 and NOEF, which probe fast motion of small amplitude, cannot give a complete description of the motional perturbation at the microphase boundary in thermoplastic elastomers. More quantitative studies concerning the lower range of the motional spectrum in the rubbery microphase need to be made in order to gain complementary insights into this perturbation.

Acknowledgment. This work was supported by the Natural Sciences and Engineering Research Council of Canada and the Quebec Ministry of Education. We thank Dr. M. T. Pham Viet and Mr. R. Mayer of this Department for their advice and help with the NMR measurements.

References and Notes

(1) Noshay, A.; McGrath, J. E. *Block Copolymers, Overview and Critical Survey*; Academic: New York, 1977; Chapter 4.
(2) Séguéla, R.; Prud'homme, J. *Macromolecules* **1978**, *11*, 1007.
(3) Haws, J. R.; Wright, R. F. In *Handbook of Thermoplastic Elastomers*; Walker, B. M., Ed.; Van Nostrand Reinhold: New York, 1979; Chapter 3.
(4) Schaefer, J. *Macromolecules* **1973**, *6*, 882.
(5) Dekmezian, A.; Axelson, D. E.; Detchter, J. J.; Borah, B.; Mandelkern, L. *J. Polym. Sci., Polym. Phys. Ed.* **1985**, *23*, 367.
(6) Dejean de la Batie, R.; Lauprêtre, F.; Monnerie, L. *Macromolecules* **1988**, *21*, 2045.
(7) Dejean de la Batie, R.; Lauprêtre, F.; Monnerie, L. *Macromolecules* **1988**, *21*, 2052.
(8) Dejean de la Batie, R.; Lauprêtre, F.; Monnerie, L. *Macromolecules* **1989**, *22*, 122.
(9) Denault, J.; Prud'homme, J. *Macromolecules* **1989**, *22*, 1307.
(10) Morèse-Séguéla, B.; St-Jacques, M.; Renaud, J. M.; Prud'homme, J. *Macromolecules* **1980**, *13*, 100.
(11) Jelinski, L. W.; Schilling, F. C.; Bovey, F. A. *Macromolecules* **1981**, *14*, 581.
(12) Blundell, D. J. *Acta Crystallogr.* **1970**, *A26*, 476.
(13) Hashimoto, T.; Shibayama, M.; Kawai, H. *Macromolecules* **1980**, *13*, 1237.
(14) Hadziioannou, G.; Skoulios, A. *Macromolecules* **1982**, *15*, 258.
(15) Helfand, E.; Wasserman, Z. R. *Macromolecules* **1976**, *9*, 879.
(16) Kraus, G.; Rollmann, K. W. *J. Polym. Sci., Polym. Phys. Ed.* **1976**, *14*, 1133.
(17) Granger, A. T.; Krause, S.; Fetters, L. J. *Macromolecules* **1987**, *20*, 1421.
(18) Krause, S.; Iskandar, M.; Iqbal, M. *Macromolecules* **1982**, *15*, 105.
(19) Gaur, U.; Wunderlich, B. *Macromolecules* **1980**, *13*, 1618.
(20) Axelson, D. E.; Russell, K. E. *Prog. Polym. Sci.* **1985**, *11*, 221.
(21) Gronski, W.; Stöppelmann, G.; Blume, A. *Polym. Prepr. (Am. Chem. Soc. Div. Polym. Chem.)* **1988**, *29* (1), 46.
(22) Doddrell, D.; Glushko, V.; Allerhand, A. *J. Chem. Phys.* **1972**, *56*, 3683.
(23) Viovy, J. L.; Monnerie, L.; Brochon, J. C. *Macromolecules* **1983**, *16*, 1845.
(24) Jones, A. A.; Stockmayer, W. H. *J. Polym. Sci., Polym. Phys. Ed.* **1977**, *15*, 847.
(25) Hall, C. K.; Helfand, E. *J. Chem. Phys.* **1982**, *77*, 3275.
(26) Connolly, J. J.; Gordon, E.; Jones, A. A. *Macromolecules* **1984**, *17*, 722.
(27) Howarth, O. W. *J. Chem. Soc., Faraday Trans. 2* **1979**, *75*, 863.
(28) Woessner, D. E. *J. Chem. Phys.* **1962**, *36*, 1.
(29) Schilling, F. C.; Cais, R. E.; Bovey, F. A. *Macromolecules* **1978**, *11*, 325.
(30) Jones, A. A.; Bisceglia, M. *Macromolecules* **1979**, *12*, 1136.
(31) Veissier, V.; Viovy, J. L.; Monnerie, L. *Polymer* **1989**, *30*, 1262.
(32) Ferry, J. D. *Viscoelastic Properties of Polymers*; Wiley: New York, 1980; Chapter 11.
(33) Törmälä, P. *J. Macromol. Sci., Rev. Macromol. Chem.* **1979**, *17*, 297.
(34) Heatley, F.; Begum, A. *Makromol. Chem.* **1977**, *178*, 1205.